Mater. Res. Soc. Symp. Proc. Vol. 1774 © 2015 Materials Research Society
DOI: 10.1557/opl.2015.732

Broad Search of Better Thermoelectric Oxides via First-Principles Computations

Qing Hao[1], Hongbo Zhao[1], Na Lu[2]
[1]Department of Aerospace and Mechanical Engineering, University of Arizona, 1130 N Mountain Ave, Tucson, AZ 85721, U.S.A.
[2]Department of Engineering Technology, University of North Carolina at Charlotte, Charlotte, NC 28223, U.S.A.

ABSTRACT

The advancement of computational tools for material property predictions enables broad search of novel materials for various energy-related applications. However, challenges still exist in accurately predicting the mean free paths (MFPs) of electrons and phonons in a high-throughput frame for thermoelectric property predictions, which largely hinders the computation-driven search for novel materials. In this work, this need is eliminated under the small-grain-size limit, in which these MFPs are restricted by the grain sizes within a bulk material. A new criterion for ZT evaluation is proposed for general nanograined bulk materials and is demonstrated with representative oxides.

INTRODUCTION

Solid-state thermoelectric (TE) devices have the ability to directly convert heat into electricity for power generation. However, the potential impact of TE technology for waste heat recovery is now hindered by the heavy usage of toxic, rare, and expensive (e.g. Te) elements. Furthermore, ultra-high-temperature (>1200 K) TE materials are still lacking due to the poor thermal stability and degraded TE performance of existing materials. For large-scale applications, it is thus of urgent need to broadly search for cost-effective TE materials for high-temperature energy harvesting. In physics, the performance of TE materials is evaluated by their TE figure of merit (ZT), defined as $ZT = S^2\sigma T/k$, where S, σ, k, and T represent Seebeck coefficient, electrical conductivity, thermal conductivity, and absolute temperature, respectively. Thermal conductivity k is sum of electron (k_E) and phonon (k_L) contributions. In previous computation-drive material search, challenges exist in accurately and effectively predicting the mean free paths (MFPs) of electrons and phonons for transport property predictions. However, this need can now be eliminated when phonon MFPs (l_P) are largely restricted by nanostructures embedded within a bulk material and the nanostructure sizes further decrease to electron MFPs (l_E). This concept is aligned with the current trend of using nanostructured bulk materials to enhance ZTs of general materials. Material search based only on electrical properties with nanograin-restricted electron MFPs is shown in [1]. In this work, the overall ZT is further predicted with this new strategy to evaluate the TE performance of various oxide compounds and alloys. Promising TE materials are identified from the investigated oxides.

THEORY: ZT ESTIMATION UNDER THE SGS LIMIT

In nanostructured materials, the optimum grain size a should satisfy $l_E<a<l_P$ to reduce k_L without deteriorating σ. The maximum ZT is anticipated when a is reduced to l_E for majority charge carriers, called the small-grain-size (SGS) limit for nanograined bulk materials [2]. In our

calculation, we assume a constant $l_P=l_E=a$. The expressions of S and σ are given by solving the Boltzmann Transport Equation (BTE):

$$\sigma = -e^2 \int \sigma(\epsilon) \left(-\frac{\partial f}{\partial \epsilon}\right) d\epsilon, \quad (1)$$

$$S = -\frac{e}{\sigma T} \int \sigma(\epsilon)(\epsilon - E_F) \left(-\frac{\partial f}{\partial \epsilon}\right) d\epsilon, \quad (2)$$

where E_F is the Fermi level, $f = 1/[1 + \exp\left(\frac{\epsilon - E_F}{k_B T}\right)]$ is the Fermi-Dirac distribution function. The function $\sigma(\epsilon)$ is related to the relaxation time $\tau_{i,\mathbf{k}}$ and group velocity $\mathbf{v}_{i,\mathbf{k}}$ for an electron state with band index i and momentum $\mathbf{k}$ within the electronic band structure. Because MFPs are limited by the grain size a, we have $\tau_{i,\mathbf{k}}=a/|\mathbf{v}_{i,\mathbf{k}}|$ and

$$\sigma(\epsilon) = \frac{1}{8\pi^3} \sum_i \int_{1BZ} \frac{a}{|\mathbf{v}_{i,\mathbf{k}}|} \left(\mathbf{v}_{i,\mathbf{k}} \cdot \hat{e}\right)^2 \delta(\epsilon - \epsilon_{i,\mathbf{k}}) d\mathbf{k}, \quad (3)$$

where ê is the unit vector of the transport direction and the integration is across the first Brillouin zone (BZ). In addition, the electronic thermal conductivity k_E is given as

$$k_E = \frac{1}{T} \int \sigma(\epsilon)(\epsilon - E_F)^2 \left(-\frac{\partial f}{\partial \epsilon}\right) d\epsilon - \frac{e^2}{\sigma T} \left(\int \sigma(\epsilon)(\epsilon - E_F) \left(-\frac{\partial f}{\partial \epsilon}\right) d\epsilon\right)^2. \quad (4)$$

As the effective values within an isotropic nanograined bulk material, above electrical properties will be averaged over x, y, and z directions for ê.

Given phonon dispersion $\omega_{i,\mathbf{q}}$ for state with branch index i and momentum $\mathbf{q}$, phonon lifetime can also be written as $\tau^p_{i,\mathbf{q}}=a/|\mathbf{v}^p_{i,\mathbf{q}}|$. Averaged over all three ê directions, the lattice thermal conductivity k_G of each grain is given by the kinetic relationship as

$$k_G = \frac{1}{N\Omega} \sum_{i,\mathbf{q}} C(\omega_{i,\mathbf{q}}) a \left|\mathbf{v}^p_{i,\mathbf{q}}\right|/3, \quad (5)$$

where N is total number of $\mathbf{q}$, Ω is volume of unit cell, C is phonon specific heat. In nanograined materials, all grains are joined by grain boundaries with a thermal resistance R_K. Based on an effective medium formulation, the effective lattice thermal conductivity k_{eff} is given as

$$k_{eff} = \frac{1}{N\Omega} \sum_{i,\mathbf{q}} \int \frac{k_L(\omega_{i,\mathbf{q}})}{1 + k_L(\omega_{i,\mathbf{q}}) R_K(\omega_{i,\mathbf{q}})/2a}. \quad (6)$$

in which $k_L(\omega_{i,\mathbf{q}}) = C(\omega_{i,\mathbf{q}}) a \left|\mathbf{v}^p_{i,\mathbf{q}}\right|/3$ and $R_K(\omega_{i,\mathbf{q}}) = 8/C(\omega_{i,\mathbf{q}}) \left|\mathbf{v}^p_{i,\mathbf{q}}\right|$ for a grain boundary [3,4]. Equation 6 simply gives $k_{\text{eff}} = 3k_G/7$ for more accurate ZT predictions.

Dividing Equations 1-6 with the common factor a, ZT of a material under the SGS limit can be computed as

$$ZT = \frac{S^2 \sigma T/a}{k_E/a + k_{\text{eff}}/a}, \quad (7)$$

which can be further optimized at a given temperature by tuning the Fermi level E_F. As a more conservative ZT estimation, optical phonons are equally treated as acoustic phonons though some high-frequency optical phonons may still have MFPs shorter than the grain size and can be overestimated for k_{eff}.

The employed electrical property calculations are carried out by modifying the package BoltzTraP [5], where a constant electron MFP is assumed for charge carriers instead of a constant relaxation time in the original code. The full-band k_{eff} calculation is similar to the electrical property calculations. Assigning a unity phonon group velocity in Equation 5, the phonon code is calibrated with specific heat computations of bulk Si and ZnO, both of which agree within 2% with the experimental data from 50 to 300 K. The electronic band structures are given by the Vienna Ab-initio Simulation Package (VASP) [6] based on the density functional theory using GGA approximation. The phonon dispersions are calculated using Phonopy package [7].

DISCUSSION

Two n-type (wurtzite ZnO, SnO_2) and two p-type oxides (ZrOS, Ca_4P_2O) as wide-bandgap electrode materials are first investigated at 1500 K. With a high melting point T_m, these materials and their nanostructures can be thermally stable during long-term operations and thus reach beyond the state-of-the-art SiGe alloys that are stable only up to ~1200 K. The selection of electrode materials for TE applications is somewhat anticipated because all existing TE materials tend to have a high room-temperature σ (~1×10^5 S/m), as suggested by the database of existing TE materials [8]. For device fabrication, such electrode materials can also form superior electrical contacts to minimize Joule heating on junctions to avoid energy loss. At 1500 K, the ZTs are plotted as a function of E_F in figures 1a. If effective p-type doping can be achieved, $ZT_{1500\,K}$ around 3 can be obtained in Ca_4P_2O.

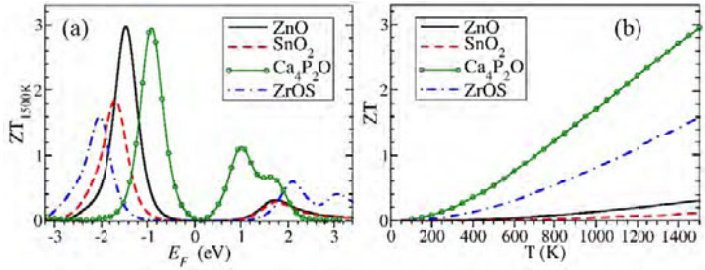

Figure 1. (a) Fermi-level (E_F) dependence of ZTs for representative oxides at 1500 K. The middle of the band gap is set to E_F=0. (b) Temperature-dependent ZTs of these oxides using the carrier concentration associated with E_F optimized at 1500 K.

Detailed information for optimized E_F and other properties is summarized in Table I. In general, maximized ZT is obtained at $|S|$ from 189 to 309 μV/K, which are higher than those to maximize $S^2\sigma$ (100-170 μV/K). The latter is comparable to the 130–187 μV/K range suggested for optimum $S^2\sigma$ of conventional materials [9]. When ZT optimization is performed at 300 K, $|S|$ will be within the 160-190 μV/K range because k_E/k_L becomes much smaller and ZT optimization can be approximated as $S^2\sigma$ optimization. The carrier concentration associated with the optimized E_F is further used to predict their temperature-dependent ZTs (figure 1b) across the whole temperature range, which monotonically increases with elevated temperatures for wide-

bandgap materials. Although high ZTs are anticipated for p-type ZnO and SnO_2, only their n-type ZTs are considered here due to the challenge in their p-type doping.

Table I: Thermoelectric properties calculated at 1500 K. ZnO and SnO_2 are n-doped and Fermi energy E_F are referenced from the conduction band bottom; Ca_4P_2O and ZrOS are p-doped and E_F are referred to the valence band top.

Material	S (μV/K)	σ/a (S m^{-1} nm^{-1})	k_{eff}/a (W m^{-1} K^{-1} nm^{-1})	k_E/a (W m^{-1} K^{-1} nm^{-1})	E_F-E_{edge} (meV)	Doping (cm^{-3})	ZT
ZnO	-188.4	5.531×10^{3}	0.947	0.159	84.5	-3.0×10^{19}	0.311
SnO_2	-189.2	5.124×10^{3}	0.853	0.139	-47.6	-2.7×10^{19}	0.277
Ca_4P_2O	308.8	1.544×10^{4}	0.420	0.328	185	2.0×10^{20}	2.95
ZrOS	280.6	1.937×10^{4}	0.866	0.568	200	1.9×10^{20}	1.60

With four atoms per primitive unit cell, wurtzite ZnO is predicted to reach $ZT_{1300\text{ K}}$=0.23 under the SGS limit. When only three acoustic branches are considered for k_{eff}, $ZT_{1300\text{ K}}$ increases to 0.66 as the upper ZT bound. The actual ZT value should be within the 0.23-0.66 range and is lower than that for bulk $Zn_{0.96}Al_{0.03}Ga_{0.01}O$ alloys ($ZT_{1247K}\approx0.65$) [10], which benefits from the electronic band structure variation of doped ZnO [11] and strong k_L reduction due to the alloy scattering of phonons. An even higher ZT is anticipated in nanograined bulk $Zn_{0.96}Al_{0.03}Ga_{0.01}O$ alloys. In general, Equation 7 can be used for fast-screening of novel materials and the obtained ZT can be improved by better designing the material.

As more general cases, eight representative oxides selected from the Inorganic Crystal Structure Database (ICSD) are optimized for their ZTs. Without the exact melting points for some oxides, all ZT optimizations are thus carried out at 800 K that is generally safe for oxides. Two new promising oxides are identified by this search. As the major p-type electrode materials [12], $AlCuO_2$ can achieve $ZT_{800\text{ K}}$>2 under the SGS limit and similarly high ZTs are also predicted for p- and n-type HfOS (figure 2).

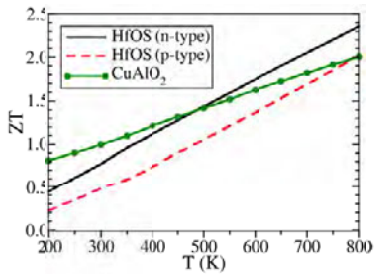

Figure 2. Temperature-dependent ZTs of p-type $AlCuO_2$ and HfOS for both types, using the carrier concentration associated with the optimized E_F at 800 K.

As general trends, the optimized $ZT_{800\,K}$ values are plotted as a function of the band gap E_g and atom number n within a primitive cell (figure 3). Figure 3a shows that the optimized ZTs may still increase when $E_g > k_B T$, in which k_B is the Boltzmann constant and T is the operation temperature. In conventional bulk materials, $E_g < 10 k_B T$ is often found [13] and ZT often decreases for wide-bandgap materials due to increased k_L. However, this rule may become invalid under the SGS limit because k_L will be largely suppressed by nanograins. Secondly, ZT monotonically increases with n (Figure 3b). As suggested earlier, $S^2\sigma$ benefits from larger n [1]. For phonons, there are 3 acoustic and 3(n-1) optical branches within a material. The fraction of optical phonons is increased for larger n and their contribution to k_{eff} is usually negligible due to their small group velocities and MFPs. This indicates that a high ZT can usually be achieved in more complicated materials.

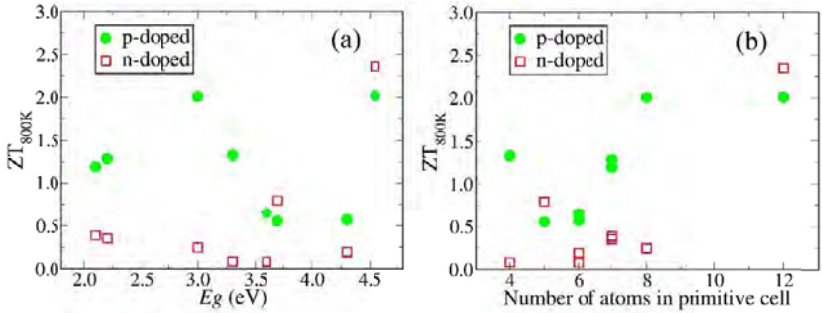

Figure 3. Optimized ZT_{800K} as a function of (a) band gap E_g and (b) number n of atoms per primitive cell.

CONCLUSIONS

In summary, a first-principles ZT evaluation of novel materials under the SGS limit is proposed in this work and demonstrated in representative oxides. This enables broad search of next-generation TE materials with low materials cost and environment beneficial. Unrestricted to oxides, the 173,473 crystal structures within the ICSD can be re-evaluated for TE applications. The materials search can be further extended to those that do not exist in nature but can be thermodynamically stable based according to their first-principles-computed formation energy [16–18]. A more general approach of non-existing material predictions can be found for batteries [19,20], which can be extended to TE materials in the future.

ACKNOWLEDGMENTS

We thank Prof. Krishna Muralidharan for sharing his VASP license with us. Na Lu thanks the support from NSF grant CMMI-1351817. An allocation of computer time from the UA Research Computing High Performance Computing (HPC) and High Throughput Computing (HTC) at the University of Arizona is gratefully acknowledged.

REFERENCES

1. S. Wang, Z. Wang, W. Setyawan, N. Mingo, and S. Curtarolo, Phys. Rev. X **1**, 021012 (2011).
2. C. Bera, M. Soulier, C. Navone, G. Roux, J. Simon, S. Volz, and N. Mingo, J. Appl. Phys. **108**, 124306 (2010).
3. Q. Hao, J. Appl. Phys. **116**, 034305 (2014).
4. Q. Hao, J. Appl. Phys. **111**, 014307 (2012).
5. G. K. H. Madsen and D. J. Singh, Comput. Phys. Commun. **175**, 67 (2006).
6. J. Hafner, J. Comput. Chem. **29**, 2044 (2008).
7. A. Togo, F. Oba, and I. Tanaka, Phys. Rev. B **78**, 134106 (2008).
8. M. W. Gaultois, T. D. Sparks, C. K. H. Borg, R. Seshadri, W. D. Bonificio, and D. R. Clarke, Chem. Mater. **25**, 2911 (2013).
9. P. Pichanusakorn and P. R. Bandaru, Appl. Phys. Lett. **94**, 223108 (2009).
10. M. Ohtaki, K. Araki, and K. Yamamoto, J. Electron. Mater. **38**, 1234 (2009).
11. S. Jantrasee, S. Pinitsoontorn, and P. Moontragoon, J. Electron. Mater. **43**, 1689 (2014).
12. H. Kawazoe, M. Yasukawa, H. Hyodo, M. Kurita, H. Yanagi, and H. Hosono, Nature **389**, 939 (1997).
13. H. J. Goldsmid, *Thermoelectric Refrigeration* (Plenum Press, New York, 1964).
14. G. A. Slack, in *Solid State Phys.*, edited by H. Ehrenreich, F. Seitz, and D. Turnbull (Academic Press, New York, 1979), pp. 1–71.
15. Z. Tian, K. Esfarjani, J. Shiomi, A. S. Henry, and G. Chen, Appl. Phys. Lett. **99**, 053122 (2011).
16. I. Opahle, G. K. H. Madsen, and R. Drautz, Phys. Chem. Chem. Phys. **14**, 16197 (2012).
17. I. Opahle, A. Parma, E. J. McEniry, R. Drautz, and G. K. H. Madsen, New J. Phys. **15**, 105010 (2013).
18. G. Hautier, A. Miglio, G. Ceder, G.-M. Rignanese, and X. Gonze, Nat. Commun. **4**, 2292 (2013).
19. L. Yang and G. Ceder, Phys. Rev. B **88**, 224107 (2013).
20. G. Hautier, C. Fischer, V. Ehrlacher, A. Jain, and G. Ceder, Inorg. Chem. **50**, 656 (2010).